Desalination and Water Treatment
Publication details, including instructions for authors and subscription information:
http://www.tandfonline.com/loi/tdwt20

Enhancement of photocatalytic activity of ZnO-SiO_2 by nano-sized Ag for visible photocatalytic reduction of Hg(II)

R.M. Mohamed [a b c] & E.S. Aazam [a]

[a] Chemistry Department, Faculty of Science, King Abdulaziz University, P.O. Box 80203, Jeddah, 21589, Saudi Arabia Phone: Tel. +966540715648 Fax: Tel. +966540715648

[b] Advanced Materials Department, Central Metallurgical R&D Institute, CMRDI, P.O. Box 87, Helwan, Cairo, 11421, Egypt

[c] Center of Excellence in Environmental Studies, King Abdulaziz University, P.O. Box 80216, Jeddah, 21589, Saudi Arabia

To cite this article: R.M. Mohamed & E.S. Aazam (2012): Enhancement of photocatalytic activity of ZnO-SiO_2 by nano-sized Ag for visible photocatalytic reduction of Hg(II), Desalination and Water Treatment, 50:1-3, 140-146

To link to this article: http://dx.doi.org/10.1080/19443994.2012.708559

Desalination and Water Treatment
www.deswater.com
50 (2012) 140–146
December

doi: 10.1080/19443994.2012.708559

Taylor & Francis
Taylor & Francis Group

Enhancement of photocatalytic activity of $ZnO–SiO_2$ by nano-sized Ag for visible photocatalytic reduction of Hg(II)

R.M. Mohamed[a,b,c,*], E.S. Aazam[a]

[a]*Chemistry Department, Faculty of Science, King Abdulaziz University, P.O. Box 80203, Jeddah 21589, Saudi Arabia*
Tel. +966540715648; Fax: +966 2 6952292; email: rmmohammed@kau.edu.sa
[b]*Advanced Materials Department, Central Metallurgical R&D Institute, CMRDI, P.O. Box 87 Helwan, Cairo 11421, Egypt*
[c]*Center of Excellence in Environmental Studies, King Abdulaziz University, P.O. Box 80216, Jeddah 21589, Saudi Arabia*

Received 6 March 2012; Accepted 4 June 2012

ABSTRACT

$ZnO–SiO_2$ nanoparticles were synthesized by a sol-gel technique from Zn $(NO_3)_2.6H_2O$ and tetraethyl orthosilicate. The synthesized samples were further modified by nano-sized Ag from silver nitrate solution through photo-assisted deposition (PAD) and impregnation (Img) routes. The obtained samples were characterized by a series of techniques including X-ray diffraction, UV–vis diffuse reflectance spectroscopy, N_2 adsorption, extended X-ray absorption fine structure, and transmission electron microscopy. The nano-sized Ag metal with a mean diameter (d) of ca. 2 nm having a narrow size distribution was found on the PAD-Ag/$ZnO–SiO_2$ catalyst, whereas the aggregated Ag metal with various sizes were observed on Img-Ag/$ZnO–SiO_2$ catalyst ($d = 12$ nm). The surface area of the synthesized samples was decreased from 550 to 480 and 350 m^2/g with $ZnO–SiO_2$, PAD-Ag/$ZnO–SiO_2$, and Img-Ag/$ZnO–SiO_2$, respectively. The UV–visible diffuse reflectance spectra spectra analysis confirmed the lowest band gap of PAD-Ag/$ZnO–SiO_2$ with a value of 2.5, compared to 2.8 and 3.2 with Img: Ag/$ZnO–SiO_2$ and $ZnO–SiO_2$, respectively. The photocatalytic reduction of Hg^{2+} to Hg^0 was performed by aqueous solution containing formic acid. The obtained results revealed that the photocatalytic activity of the prepared samples increased in the order; $ZnO–SiO_2$ < Img-Ag / $ZnO–SiO_2$<PAD-Ag/$ZnO–SiO_2$. The surface area decreased from 550 to 480 and 450 m^2/g, while the efficiency of the photocatalytic reduction Hg (II) increased from 30 to 73 and 100%, with the $ZnO–SiO_2$, Img-Ag/$ZnO–SiO_2$ and PAD-Ag /$ZnO–SiO_2$ samples, respectively.

Keywords: ZnO/SiO_2; Ag loading; Activity enhancement; Visible photocatalysis; Hg (II)

1. Introduction

Mercury (II) is a frequent component of industrial wastewaters and is used in agricultural products such as pesticides, fungicides, herbicides, insecticides, and bactericides, which are currently forbidden. Mercury is also used in other industries (e.g. chlorine–alkali, paints, pharmaceuticals, electronics, cosmetics, etc.) [1,2]. In aquatic systems, mercury is often converted by bacteria into methyl mercury, being magnified hundreds to thousands of times as it moves through the aquatic food chain, posing a potential risk to humans and wildlife that consume fish [3]. Heterogeneous photocatalysis is a convenient tool for mercury

*Corresponding author.

reduction because it uses inexpensive chemicals [4] and due to the potential use of sunlight as the energy source the catalyst can be recycled many times without significant loss of activity.

Zinc Oxide (ZnO) is an n-type semiconductor with a wide direct band gap of 3.37 eV. Recently, much effort has been devoted to study ZnO as a promising photocatalyst for photocatalytic degradation of water pollutants, owing to its high activity, low cost, and environmentally friendly feature [5–8]. ZnO present as nano-scale particles has a high surface area to volume ratio and provides more active sites on the surface and therefore increases the rate of reaction on its surface such as for photocatalytic degradation [9]. However, a major drawback of ZnO is the large band gap of 3.37 eV, so wavelengths below 400 nm are necessary for excitation. Another disadvantage of ZnO is that charge carrier recombination of photo-generated electron/hole pairs occurs within nanoseconds and the photocatalytic activity is low [10–13]. Therefore, it is necessary to improve its visible-light activities by extending its absorption threshold from the UV light region to the visible light region and also to reduce the recombination of photo-generated electron/hole. Different attempts were made recently to improve the activity of ZnO catalyst. Development of core/shell structured materials on a nanometer scale has been receiving extensive attention [14,15]. The shell can alter the charge, functionality, and reactivity of surface, or improve the stability and dispersive ability of the core material. Furthermore, catalytic, optical, or magnetic functions can be imparted to the core particles by the shell material. In general, the synthesis of core/shell structured material has the goal of obtaining a new composite material having synergetic or complementary behaviors between the core and shell materials. Many studies on the synthesis of composites such as; NiO [16], V_2O_5 [17], TiO_2 [18], Fe_2O_3 [19], and Pt [20] coated with SiO_2 shells have been reported. SiO_2 is a most studied shell candidate due to its relative ease in preparation, good environmental stability, and compatibility with other materials, which motivated the synthesis of the core/shell-structured composite of ZnO and SiO_2 and expected to achieve novel properties resulting from the synergic interaction of these two chemical components. One of the most promising methods to increase the photocatalytic efficiency is surface modification of ZnO; this can be achieved by metal doping into the ZnO catalyst. Dopant can act as a sink to collect photogenerated electrons from the conduction band of the semiconductor. Thus, it hinders the recombination of photogenerated electrons and holes through increasing the charge separation [21–24]. The surface modification of ZnO nanoparticles by preparing charge-transfer catalysts with mixing multi-component oxides can enhance the surface chemical and physical properties and considered as the key for the successful photocatalytic applications of such nanoparticles. Several metal ions such as Fe [25] have been used as dopants for ZnO to improve its photocatalytic activity.

In the present work, Ag/ZnO–SiO_2 nanoparticles with large specific surface areas were synthesized by the application of a photo-assisted deposition (PAD) and impregnation (Img) methods, and the properties of the nanoparticles were characterized by X-ray diffraction (XRD), transmission electron microscopy (TEM), Extended X-ray absorption fine structure (EXAFS), UV–visible diffuse reflectance spectra (UV–vis/DRS), and BET analysis. The photocatalytic activity of the synthesized nanoparticles was evaluated by the photocatalytic reduction of Hg (II) under visible irradiation.

2. Experimental methods

2.1. Chemicals

Zn $(NO_3)_2.6H_2O$, $AgNO_3$ and tetraethyl orthosilicate (TEOS) were purchased from Aldrich and selected as the precursors of zinc, silver, and silica, respectively. $HgCl_2$ (mercury (II) chloride) was purchased from Merck with 99.5% purity. All chemicals used in this work were of reagent-grade quality. The water used was deionized water.

2.2. Preparation of ZnO–SiO_2

ZnO–SiO_2 nanoparticles were synthesized via a sol-gel technique. In a typical procedure, 20 ml TEOS was mixed with ethyl alcohol (C_2H_5OH), ultra pure water (H_2O), and nitric acid (HNO_3) under vigorous stirring for 1 h. The overall molar ratio of TEOS: C_2H_5OH: H_2O: HNO_3 was 1: 4: 8: 0.02. An aqueous solution of $Zn(NO_3)_2.6H_2O$ was added into the above solution under vigorous stirring for 60 min. The prepared samples were aged for 24 h. Finally, the samples were evaporated and dried at 80°C, followed by calcination at 550°C for 3 h in air.

2.3. Preparation of Ag loaded on ZnO–SiO_2 using PAD method

Ag metal (4 wt.%) was deposited on ZnO–SiO_2 from aqueous solution of $AgNO_3$ irradiated by UV-light irradiation (Xenon lamp) for 24 h. The samples were dried at 100°C and reduced by H_2 (20 ml/min) at 350°C for 4 h to confirm complete reduction of Ag to Ag^0.

2.4. Preparation of Ag loaded on ZnO–SiO_2 using Img method

In a typical Img method, the 4 wt.% of Ag metal was deposited by a simple Img of ZnO–SiO_2 in the absence of light with aqueous solution of $AgNO_3$. The samples were dried at 100°C and reduced by H_2 (20 ml/min) at 350°C for 4 h.

2.5. Characterization techniques

To determine the crystallite sizes and identities of the Ag-loaded on ZnO–SiO_2 nanocomposite photocatalyst, XRD analysis was carried out at room temperature using Rigaku X-Ray diffractometer with Cu Kα ($\lambda = 1.540$ Å) radiation over a 2θ collection range of 10–80°. The shape of the samples were tested using Hitachi H-9500 TEM, the prepared samples was synthesized by suspending the samples in ethanol, followed by ultrasonication for 30 min, then a small amount of this solution onto a carbon-coated copper grid, and drying before loading the sample in the TEM. Specific surface area was calculated from measurements of N_2-adsorption using Nova 2000 series Chromatech apparatus at 77 K. Prior to the measurements all samples were treated under vacuum at 200°C for 2 h. Bandgap of the samples was identified by UV–vis–DRS in air at room temperature in the wavelength range 200–800 nm using Shimadzu UV-2450 spectrophotometer. The EXAFS is performed at beam line7 C facility [26] of the Photon Factory at the National Laboratory for High Energy Physics, Tsukuba, Tokyo, Japan.

2.6. Photocatalytic experiment

2.6.1. Photoreduction

Stock solutions of Hg (II) (120 mg mL^{-1}) were prepared from a Merck (99.5%) $HgCl_2$ (mercury (II) chloride) solution in water. The reaction mixture was kept in a reactor with a cylindrical Pyrex cell of 1,000 cm^3, and 500 cm^3 of a Hg (II) solution of a given concentration was added to 1 g of the photocatalyst. The solution pH was adjusted to 4.0 with formic acid. The reaction was conducted with the reactor open to air and oxygen stream bubbled in the suspension at 0.5 cm^3/min. A 125-W medium pressure mercury lamp with UV cut filter, surrounded by a quartz thimble, was used for irradiation. In order to maintain the room temperature (~20°C), the vessel was surrounded by a water jacket with an inlet and an outlet for the passage of cold water. The reactor contained a magnetic stirrer to maintain the reaction mixture homogeneous. At regular intervals, 6-cm^3 aliquots of the suspension were withdrawn and filtered through a 0.45-μm Millipore filter. The concentration of mercury (II) in solution was determined by a Spectra AA—10 Plus VARIAN spectrophotometer.

The photocalytic reduction efficiency of Hg^{2+} was estimated by applying the following equation:

$$\%\ \text{Photocalytic reduction of } Hg^{2+} = (C_o - C)/C_o \times 100$$

where C_o is the initial concentration of Hg^{2+}, and C is the residual Hg^{2+} concentration in solution.

2.6.2. Adsorption

In order to verify the adsorption capacity, experiments without a mercury lamp were developed. The reaction mixture was kept in a reactor with a cylindrical Pyrex cell in 1,000 cm^3 of water; 500 cm^3 of a Hg (II) solution of a given concentration was added to 1 g of the photocatalyst. The reactor was open and an air and oxygen stream was bubbled in the suspension at 0.5 cm^3/min. The reactor contained a magnetic stirrer to maintain the homogeneity of the reaction mixture. At regular intervals, a 6-cm^3 aliquot of the suspension was withdrawn and filtered through a 0.45-μm Millipore filter. The concentration of Hg(II) in the solution was determined by a SpecrtAA—10 Plus VARIAN spectrophotometer, which was used for all spectrophotometric measurements (wavelength 253.7).

The adsorption efficiency of Hg^{2+} was estimated by applying the following equation:

$$\%\ \text{adsorption efficiency of } Hg^{2+} = (C_o - C)/C_o \times 100$$

where C_o is initial concentration of Hg^{2+}, and C is the residual Hg^{2+} concentration in solution.

3. Results and discussion

3.1. Phase analysis

The XRD patterns of the ZnO–SiO_2 and Ag doped ZnO–SiO_2 nanoparticles prepared by (Img) and (PAD) routes are shown in Fig. 1. It can be seen that the diffraction patterns of ZnO–SiO_2 sample and all Ag-doped ZnO–SiO_2 are mainly composed of ZnO phase which still exists after applying both above-mentioned preparation methods. While, in the Ag-doped samples; no diffraction peaks of Ag were observed, this is probably attributed to the low Ag doping content (ca. 4 wt.%). Moreover, it is obvious that, Ag is well

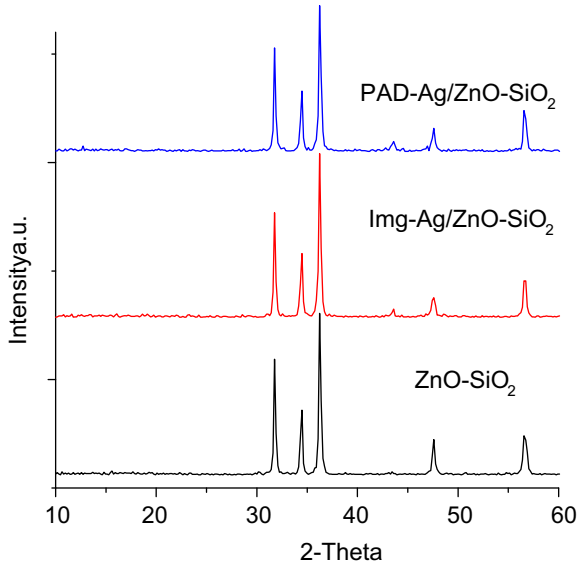

Fig. 1. XRD patterns of the ($ZnO–SiO_2$, Img-Ag/$ZnO–SiO_2$, and PAD-Ag/$ZnO–SiO_2$).

dispersed over the $ZnO–SiO_2$ surface, which was confirmed by TEM as mentioned in the catalyst characterization part.

3.2. Catalyst characterization

The Fourier transforms of Pt LIII-edge EXAFS spectra of the Ag-loaded catalysts are shown in Fig. 2. The presence of the peak assigned to the Ag–Ag bond of Ag metal at around 2.86 Å indicates the formation of nano-sized Ag metal [27]. The intensity of the Ag–Ag peak of the PAD-Ag/ZnO–SiO_2 catalyst is smaller than the imp-Ag/ZnO–SiO_2 catalyst. Ag metal particles formed on the photo-deposited catalyst (PAD-Ag/ZnO–SiO_2) show smaller particle size than that of the impregnated catalyst (imp-Ag/ZnO–SiO_2). These findings suggest that the size of Ag metal particles depends on the preparation method.

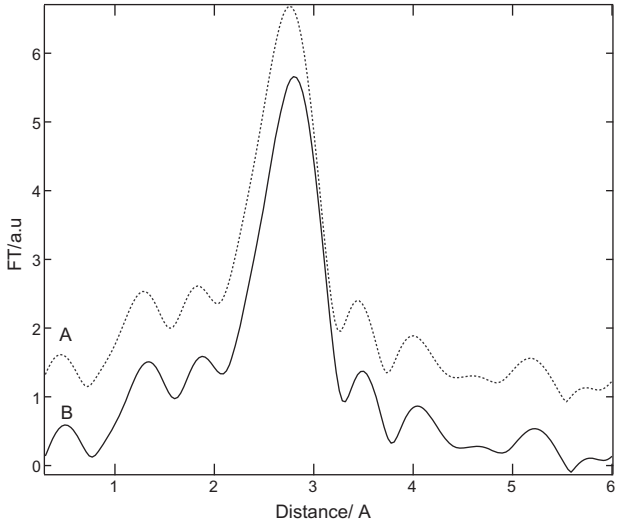

Fig. 2. Fourier transforms of the Pt L_{III}-edge EXAFS spectra for Img-Ag/$ZnO–SiO_2$ (A) and PAD-Ag/$ZnO–SiO_2$ (B).

The grain sizes of PAD-Ag/$ZnO–SiO_2$ and Img-Ag/$ZnO–SiO_2$ nanocomposite photocatalysts were displayed in TEM images as shown in Fig. 3. The particle size distribution obtained from the analysis of TEM images is shown in Fig. 4. The results reveals that the nano-sized Ag metal with a mean diameter (d) of ca. 2 nm having a narrow size distribution was found on the PAD-Ag/$ZnO–SiO_2$ catalyst, whereas the aggregated Ag metal within various sizes is observed on Img-Ag/$ZnO–SiO_2$ catalyst ($d = 12$ nm) which is in agreement with the results of EXAFS measurement. These findings suggest that the size of Ag metal particles depends on the preparation method. Also, TEM micrographs showed the homogenous distribution of Ag over $ZnO–SiO_2$ matrix which were prepared by PAD method.

3.3. Surface area analysis

Specific surface area (S_{BET}) of $ZnO–SiO_2$, PAD-Ag/$ZnO–SiO_2$, and Img-Ag/$ZnO–SiO_2$ powder samples were determined. The S_{BET} values were 550, 480, and 450 m^2/g for the $ZnO–SiO_2$, Img-Ag/$ZnO–SiO_2$, and PAD-Ag/$ZnO–SiO_2$, respectively. The parameters of surface area and the data calculated from the t-plot are collected in Table 1. Furthermore, the total pore volume of $ZnO–SiO_2$ is higher than that of Ag-ZnO–SiO_2 due to the blocking of some pore by deposition of Ag metal. The values of S_{BET} and S_t are generally close in most samples indicating the presence of mesopores.

3.4. Band-gap analysis (UV–vis–DRS)

Study of the UV–visible radiation absorption is an important tool for evaluating the changes in the absorbance spectra of the prepared semiconductor materials. This is expressed by the band-gap (E_g) measurement which can be altered by different parameters. For instance, E_g value for pure ZnO phase is usually reported 3.37 [7], however these values are influenced by the synthesis method, and also affected by the existence of impurities doping the crystalline

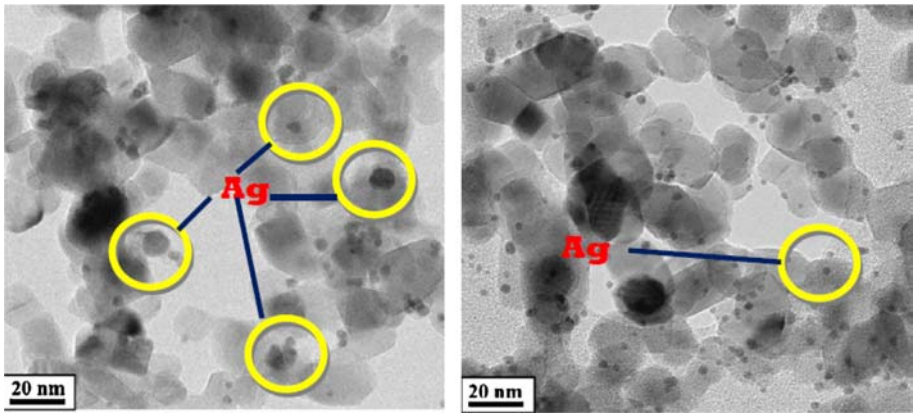

Fig. 3. The TEM images of the Img: Ag/ZnO–SiO_2 (left) and PAD-Ag/ZnO–SiO_2 (right) catalysts.

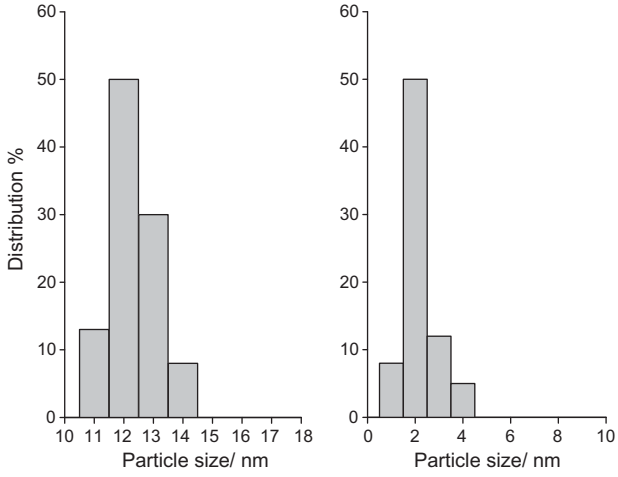

Fig. 4. Size distribution diagrams of Ag metal obtained from the TEM images of the Img-Ag/ZnO–SiO_2 (left) and PAD-Ag/ZnO–SiO_2 (right) catalysts.

network and also the average crystal size of the semiconductor. In a previous study, different methods for calculating the E_g from the UV–Vis reflectance spectra were used. For example, some authors calculated the E_g values by a direct extrapolation of the F(R) spectrum whereas others reported the wavelength corresponding to the maximum absorption [28]. As a consequence, quite different E_g values for ZnO samples are found in the literature. For instance, a threshold wavelength values of 240 nm [28], 290 nm [29], and 360 nm [30] corresponding to band gaps 5.15, 4.28, and 3.45, respectively. Fig. 5 gives UV–vis–DRS of (ZnO–SiO_2, Img-Ag/ZnO–SiO_2 and PAD-Ag/ZnO–SiO_2). The results showed an increase in the absorbance in the visible light region with the Ag doping. The values of E_g for the synthesized semiconductors can be derived from the spectra by plotting $(F(R)\cdot h\gamma)^{1/2}$ against $h\gamma$. The results revealed that the calculated values of E_g for (ZnO–SiO_2, Img-Ag/ZnO–SiO_2 and PAD-Ag/ZnO–SiO_2) were 3.2, 2.8, and 2.5 eV, respectively. This indicates shifting the spectra of the PAD-Ag/ZnO–SiO_2 and Img-Ag/ZnO–SiO_2 samples to the visible light area.

Table 1
Texture parameters of ZnO–SiO_2, Img-Ag/ZnO–SiO_2 and PAD-Ag/ZnO–SiO_2

Sample	S_{BET} (m^2/g)	S_t (m^2/g)	S_{micro} (m^2/g)	S_{ext} (m^2/g)	V_p (cm^3/g)	V_{micro} (cm^3/g)	V_{meso} (cm^3/g)	r (Å)
Img-Ag/ZnO–SiO_2	450	365	310	140	0.677	0.077	0.600	39.00
PAD-Ag/ZnO–SiO_2	480	470	300	180	0.788	0.044	0.744	38.00
ZnO–SiO_2	550	520	350	200	0.888	0.070	0.810	36.00

Notes: S_{BET}: BET-surface area.
S_t: surface area derived from V_{1-t} plots.
S_{mic}: surface area of micropores.
S_{ext}: external surface area.
V_p: total pore volume.
V_{mic}: pore volume of micropores.
V_{mes}: pore volume of mesopores.
r^-: mean pore radius.

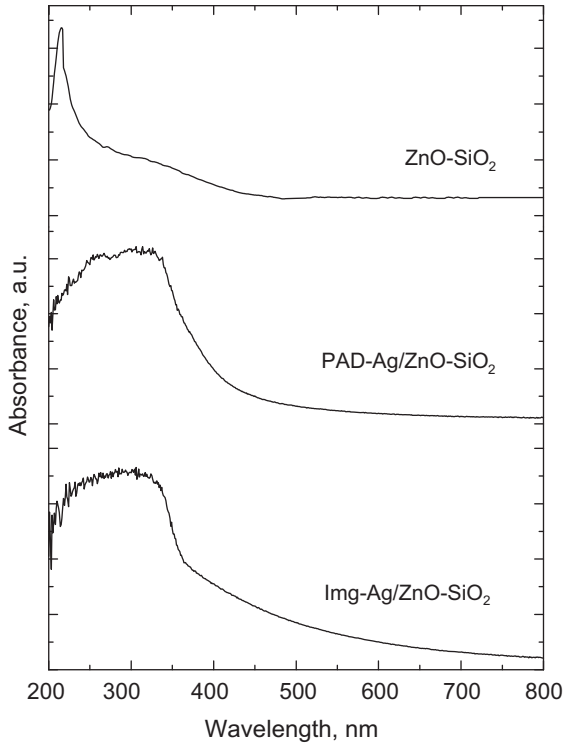

Fig. 5. Diffuse reflectance UV–Vis absorption spectra of $ZnO–SiO_2$, Img-Ag/$ZnO–SiO_2$, and PAD-Ag/$ZnO–SiO_2$.

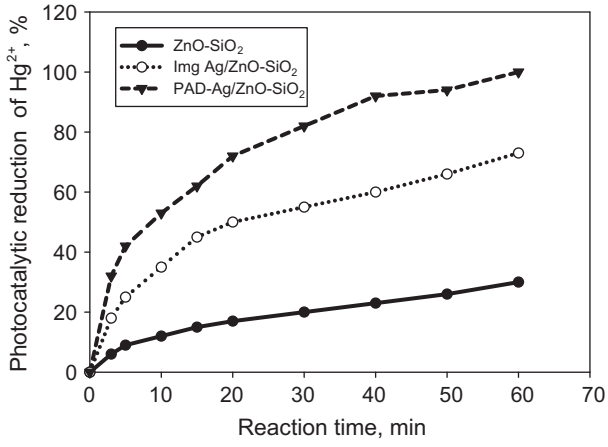

Fig. 6. Photocatalytic reduction of Hg^{2+} (%) for $ZnO–SiO_2$, Img-Ag/$ZnO–SiO_2$, and PAD-Ag/$ZnO–SiO_2$.

3.5. Evaluation of photocatalytic activity

Fig. 6 displays the photocatalytic reduction of Hg^{2+} of 120 mg/l Hg^{2+} pertaining to ($ZnO–SiO_2$, Img-Ag/$ZnO–SiO_2$ and PAD-Ag/$ZnO–SiO_2$) at solution pH 4 for different time intervals. It can be seen that the rate of Hg^{2+} photoreduction increased gradually with time; reaching maximum efficiency values of 30, 73, and 100% after 1 h with parent $ZnO–SiO_2$, Img-Ag/$ZnO–SiO_2$, and PAD-Ag/$ZnO–SiO_2$ samples, respectively. Considering that, the pure Ag oxides has no photocatalytic oxidation properties, such change in the photodegradation activity may be explained in terms of the differences in interaction between Ag and $ZnO–SiO_2$ that led to several modifications in physical properties such as band gap, particle size, and surface texture. Also, one could observe that, the catalytic activity of $ZnO–SiO_2$ generally increased with the addition of Ag promoters. It was obvious that the photoreduction activity was gradually increased with the decrease of band gap and the increase of the active site. It is believed that the lack of electron scavengers (surface Zn^{2+}) and hole traps (surface hydroxyl groups) is responsible for the rapid recombination rate of e^-/h^+, which leads to lower photocatalytic activity with the parent $ZnO–SiO_2$ sample [6–9]. The photocatalytic activities of the Ag-doped $ZnO–SiO_2$ nanoparticles increased due to that Ag plays two important roles; lowering the energy of electron excitation from valance band to conduction band, and hindering the rate of e^-/h^+ recombination. Thus it lowered both the band gap (as confirmed from the UV–vis–DRS spectra analysis) and particle size (as confirmed from the TEM analysis).

Also, the adsorption experiments reveal that the adsorption efficiency % in the case of $ZnO–SiO_2$, Img-Ag/$ZnO–SiO_2$,and PAD-Ag/$ZnO–SiO_2$ is 22, 15 and 10%, respectively. Therefore, in the case of Img-Ag/$ZnO–SiO_2$ and PAD-Ag/$ZnO–SiO_2$ % of Hg^{2+} removal is a photocatalytic reduction not an adsorption process. But in the case of $ZnO–SiO_2$, % of Hg^{2+} removal is adsorption not photocatalytic reduction.

4. Conclusions

Ag doping, through PAD and Img routes, can greatly enhance the performance of $ZnO–SiO_2$ as a photocatalyst. The nano-sized Ag metal with a mean diameter (d) of ca. 2 nm having a narrow size distribution was found on the PAD-Ag/$ZnO–SiO_2$ catalyst, whereas the aggregated Ag metal with various sizes are observed on Img-Ag/$ZnO–SiO_2$ catalyst ($d = 12$ nm). The surface area of the synthesized samples was decreased from 550 to 480 and 350 m^2/g with $ZnO–SiO_2$, PAD-Ag/$ZnO–SiO_2$, and Img-Ag/$ZnO–SiO_2$, respectively. The UV–vis–DRS spectra analysis confirmed the lowest band gap of PAD-Ag/$ZnO–SiO_2$ with a value of 2.5, compared to 2.8 and 3.2 with Img: Ag/$ZnO–SiO_2$ and $ZnO–SiO_2$, respectively. The photocatalytic reduction of Hg^{2+} was found to be much more effective in the PAD-Ag/$ZnO–SiO_2$. The reduction efficiency increased from 30 to 73 and 100%, with the ZnO/SiO_2, Img-Ag/$ZnO–SiO_2$ and PAD-Ag/$ZnO–SiO_2$ samples, respectively. The smallest particle

size and lowest band gap of the PAD-Ag/ZnO–SiO_2 sample lead to the highest photocatalytic activity with Hg^{2+} reduction.

References

[1] E.M. Fournière, A.G. Leyva, E.A. Gautier, M.I. Litter, Treatment of phenyl mercury salts by heterogeneous photocatalysis over TiO_2, Chemosphere 69 (2007) 682–688.

[2] J. Barron-Zambrano, S. Laborie, Ph. Viers, M. Rakib, G. Durand, Mercury removal from aqueous solutions by complexation–ultrafiltration, Desalination 144 (2002) 201–206.

[3] N. Serpone, Y.K. Ah-You, T.P. Tran, R. Harris, E. Pelizzetti, H. Hidaka, AM1 simulated sunlight photoreduction and elimination of Hg(II) and CH_3Hg(II) chloride salts from aqueous suspensions of titanium dioxide, Sol. Energy 39 (1987) 491–498.

[4] N. Serpone, E. Borgarello, E. Pelizzetti, Photoreduction and photodegradation of inorganic pollutants: II. Selective reduction and recovery of Au, Pt, Pd, Rh, Hg, and Pb, in: M. Schiavello (Ed.), Photocatalysis and Environment, Kluwer Academic, Dordrecht, 1988, p. 527.

[5] M. Nasr-Esfahani, A. Khakifirooz, N. Tavakoli, M.H. Soleimani, Preparation, characterization and photocatalytic activity of a novel nanostructure ZnO composite film derived sol–gel process using organic binder materials, Desalin. Water Treat. 21 (2010) 202–209.

[6] B.H. Hameed, U.G. Akpan, Keng Poh Wee, Photocatalytic degradation of Acid Red 1 dye using ZnO catalyst in the presence and absence of silver, Desalin. Water Treat. 27 (2011) 204–209.

[7] S. Lam, J. Sin, A. Zuhairi Abdullah, A. Mohamed, Degradation of wastewaters containing organic dyes photocatalyzed by zinc oxide: A review, Desalin. Water Treat. 41 (2012) 131–169.

[8] X. Liu, T. Lv, L. Pan, Z. Sun, C. Sun, Microwave assisted synthesis of ZnO with Photocatalytic reduction of Cr (VI) in aqueous solution, Desalin. Water Treat. 40 (2012) 24–32.

[9] C. Hariharan, Photocatalytic degradation of organic contaminants in water by ZnO nanoparticles: Revisited, Appl. Catal. A: Gen. 304 (2006) 55–61.

[10] M. Mrowetz, E. Selli, Photocatalytic degradation of formic and benzoic acids and hydrogen peroxide evolution in TiO_2 and ZnO water suspensions, J. Photochem. Photobiol. A: Chem. 180 (2006) 15–22.

[11] T. Pauporte, J. Rathousky, Electrodeposited mesoporous ZnO thin films as efficient photocatalysts for the degradation of dye pollutants, J. Phys. Chem. C 111 (2007) 7639–7644.

[12] J. Yu, X. Yu, Hydrothermal synthesis and photocatalytic activity of zinc oxide hollow spheres, Environ. Sci. Technol. 42 (2008) 4902–4907.

[13] J.H. Sun, S.Y. Dong, Y.K. Wang, S.P. Sun, Preparation and photocatalytic property of a novel dumbbell-shaped ZnO microcrystal photocatalyst, J. Hazard. Mater. 172 (2009) 1520–1526.

[14] M. Zhou, J. Yu, B. Cheng, Effects of Fe-doping on the photocatalytic activity of mesoporous TiO_2 powders prepared by an ultrasonic method, J. Hazard. Mater. B 137 (2006) 1838–1847.

[15] C. Klingshirn, ZnO: Material, physics and applications, Chem. Phys. Chem. 8 (2007) 782–803.

[16] A. Singhal, S. Achary, A. Tyagi, P. Manna, S. Yusuf, Colloidal Fe-doped ZnO nanocrystals: Facile low temperature synthesis, characterization and properties, Mater. Sci. Eng. B 153 (2008) 47–52.

[17] C. Estrellan, C. Salim, H. Hinode, Photocatalytic activity of sol–gel derived TiO_2 co-doped with iron and niobium, React. Kinet. Catal. Lett. 98 (2009) 187–192.

[18] J.J. Schneider, Synthesis of ZnO nanocrystals with cone, hexagonal cone, and rod shapes via non-hydrolytic ester elimination Sol–Gel reactions, Adv. Mater. 13 (2001) 529–533.

[19] H.B. Lee, Y.M. Yoo, Y.H. Han, Characteristic optical properties and synthesis of gold–silica core–shell colloids, Scr. Mater. 55 (2006) 1127–1129.

[20] R.M. Mohamed, E.S. Aazam, Photocatalytic oxidation of carbon monoxide over NiO/SnO2 nanocomposites under UV Irradiation, J. Nanotechnol. (2012) Art. no. 794874.

[21] A.A. Ismail, I.A. Ibrahim, R.M. Mohamed, Sol–Gel Synthesis of Vanadia –silica for photocatalytic degradation of cyanide, Appl. Catal. B: Environ. 45(2) (2003) 161–166.

[22] J. Zhang, Z. Liu, B. Han, Z. Li, G. Yang, J. Li, J. Chen, Preparation of silica and TiO_2–SiO_2 core–shell nanoparticles in water-in-oil microemulsion using compressed CO_2 as reactant and antisolvent, J. Supercrit. Fluids 36 (2006) 194–201.

[23] V. Maurice, T. Georgelin, J.M. Siaugue, V. Cabuil, Synthesis and characterization of functionalized core–shell γ-Fe_2O_3–SiO_2 nanoparticles, J. Magn. Magn. Mater. 321 (2009) 1408–1413.

[24] R.M. Mohamed, Characterization and catalytic properties of nano-sized Pt metal catalyst on TiO_2-SiO_2 synthesized by photo-assisted deposition and impregnation methods, J. Mater. Process. Technol. 209(1) (2009) 577–583.

[25] M. Height, S. Pratsinis, O. Mekasuwandumrong, P. Praserthdam, Ag-ZnO catalysts for UV-photodegradation of methylene blue, Appl. Catal. B: Environ. 63 (2006) 305–312.

[26] R. Ullah, J. Dutta, Photocatalytic degradation of organic dyes with manganese-doped ZnO nanoparticles, J. of Hazard. Mater. 156 (2008) 194–200.

[27] P.R. Sarode, K.R. Priolka, B. Bera, M.S. Hegda, S. Emura, R. Kumashiro, Study of local environment of Ag in Ag/CeO_2 catalyst by EXAFS, Mater. Res. Bull. 37 (2002) 1679–1690.

[28] R.M. Mohamed, M.A. Al-Rayyani, E.S. Baeissa, I.A. Mkhalid, Nano-sized Fe-metal catalyst on ZnO–SiO_2: (photo-assisted deposition and impregnation) Synthesis routes and nanostructure characterization, J. Alloys Compd. 509(24) (2011) 6824–6828.

[29] N. Masaharu, K. Atsushi, Design of an XAFS beamline at the photon factory: Possibilities of bent conical mirrors, J. Synchrotron Radiat. 6 (1999) 182–184.

[30] R.M. Mohamed, E.S. Aazam, Preparation and characterization of platinum doped porous titania nanoparticles for photocatalytic oxidation of carbon monoxide, J. Alloys Compd. 509 (2011) 10132–10138.